Electronic Supplementary Material (ESI) for RSC Advances.

Electronic Supplementary Information

Electronic performance of printed PEDOT:PSS lines correlated to the physical and chemical properties of coated inkjet papers

Viviane Forsberg *[a,b,c], Jan Mašlík [d] and Magnus Norgren [a]

Atomic percentages of the mapping and principal X-ray lines for the EDS analyses

Table S1 Principal X-ray emission lines in KeV

Energy level	C	O	Ca	Cl	Si	Al	Cr	Ti
K α	0.2774	0.5249	3.6905	2.6219	1.7398	1.4866	5.4117	4.5089

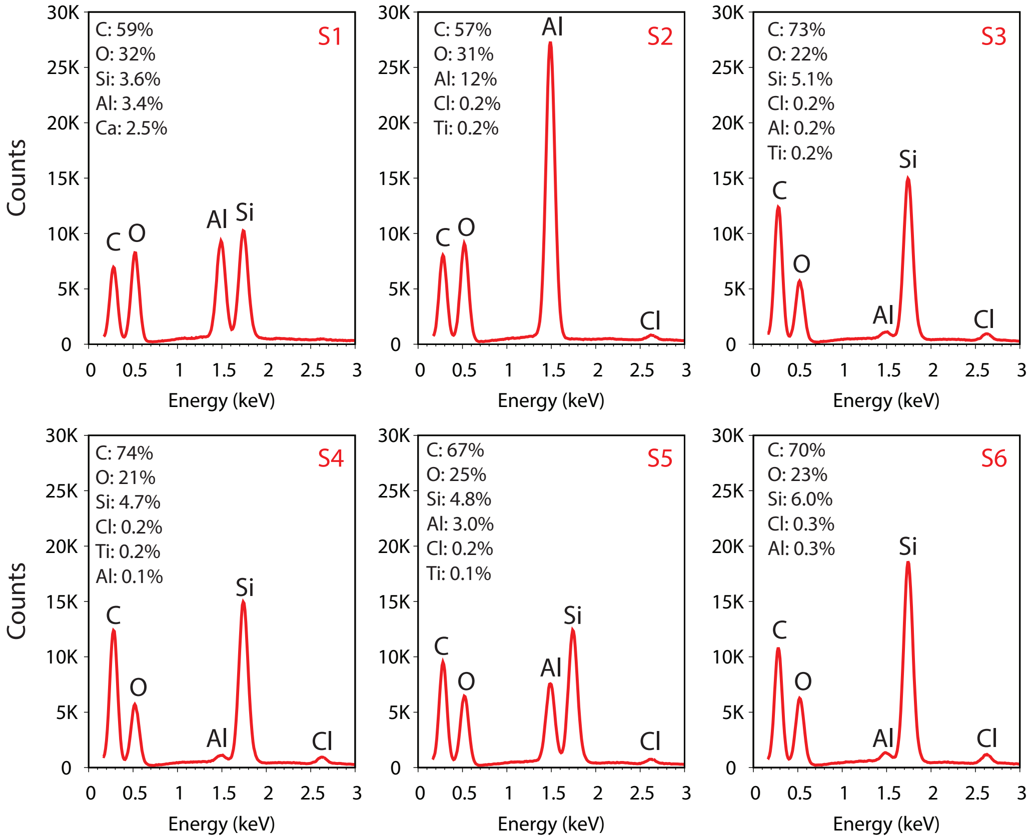

Fig. S1 EDS data from the surface mapping of the entire surface of the cross section of the embedded substrates where the SEM images and EDS graphical results are presented in the main paper at Fig. 3

---

[a] *Mid Sweden University, FSCN, Surface and Colloid Engineering, Holmgatan 10, SE-851 70, Sundsvall, Sweden. Email: viviane.forsberg@miun.se*

[b] *KTH Royal Institute of Technology, Department of Fiber and Polymer Technology, Biocomposites division, Teknikringen 56, SE-100 44, Stockholm, Sweden. E-mail: vivforsb@kth.se*

[c] *Wallenberg Wood Science Centre, Teknikringen 56, SE-100 44, Stockholm, Sweden*

[d] *Tomas Bata University in Zlín, Centre of Polymer Systems, Trida Tomase Bati 5678, CZ-760 01, Zlín, Czech Republic*

Thin film transistors

TFTs with the hole and electron mobility in the range of amorphous silicon mobility $1\,\mathrm{cm^2\,V^{-1}\,s^{-1}}$ for organic conjugated polymers like PEDOT:PSS have been demonstrated[1]. With somewhat lower charge carrier mobilities of $0.087\,\mathrm{cm^2\,V^{-1}\,s^{-1}}$, printed TFTs on paper were reported[2], as well as paper-based actuators[3], but a screen-like application printed on paper has not yet been achieved. The development of organic electronics could enable applications such as electronic paper, but to achieve that, it is necessary to print transistors with sub-micron switching channels, which can be achieved by surface energy patterns combining electron beam lithography and inkjet printing[4]. However, that has not been achieved yet with fully printed electronics due to the limited resolution of inkjet printing (i.e., $25\,\mu\mathrm{m}$) and other depositing techniques[5].

Spatial resolution of FTIR versus Raman spectroscopy

Firstly, let us discuss the resolution of the FTIR and Raman instruments we used. This is important because the penetration depth of the evanescent wave (δ) will dictate how far into the IRL the instrument would detect the elemental composition with precision. To distinguish well two points in microscopy, the smallest distance δ should be double for a high-quality microscopy image[6].

$$\delta = \frac{1.22\lambda}{2n\ sin\theta} = \frac{0.61}{\lambda/NA} \tag{S1}$$

For mid-IR wavelengths the FTIR spectrum is $2.7\,\mu\mathrm{m}$ at $3600\,\mathrm{cm^{-1}}$ and $8\,\mu\mathrm{m}$ at $1240\,\mathrm{cm^{-1}}$. Which correspond to a spatial resolution of 5 and $16\,\mu\mathrm{m}$ respectively. This becomes important in our study because there are CLs as thin as $0.5\,\mu\mathrm{m}$, which goes beyond the detection upper limit of $16\,\mu\mathrm{m}$ creating a misleading interpretations of the results without the help of the EDS because there were multiple layers present in the substrate that we could only identify with the cross-section image and the further EDS analyses.

It is important to highlight that Raman is a scattering technique while FTIR is an absorption technique, the use of one or the other technique is based on the lateral resolution required and the type of functional group of interest[6]. To estimate the spatial resolution of Raman we can also employ Eq. S1, where NA is the numerical aperture of the objective (i.e., $0.90/100x$), n is the refractive index and θ is half the angular aperture, giving for our system δ=$360\,\mathrm{nm}$.

Raman spectroscopy have higher spectral resolution as we presented in our calculations, the bands are narrower and less susceptible to spectral interference than FTIR but for photosensitive samples the resolution is hindered as we need to use lower laser power to not damage the sample and to minimize fluorescence. FTIR will enable access to a wider range of functional groups[6]. The fluorescence could be minimized to some extent by varying the parameters such as slit opening, grating, laser power and acquisition time (i.e., short times), number of accumulations (i.e., multiple accumulations) or by using an excitation wavelength in the near IR region (i.e., $785\,\mathrm{nm}$)[7]. The detectability of the EDS measurement was evaluated from the background analysis versus the peak height, and it was related to FTIR results for the outermost layers.

Surface energy of the substrates

Through the measurement of the contact angle of liquids with known parameters of the three-components surface energy method proposed by Van Oss[8] for the interfacial Lifshitz-van der Waals (LW) and polar interactions (AB), we identified monopolar substrates indicating surfaces with relatively high affinity to dipole-dipole, induced dipole or hydrogen bonding to wetting liquids.

The theory behind the Lifshitz-van der Waals (the dispersive or apolar component of the surface tension) and acid-base (the polar component of the surface tension) is well described in the literature[8]. A simplified version of these equations can be found in the literature[9]. The acid component or electron donor, indicates how a surface is favorable to specific interactions such as dipole-dipole, induced dipole or hydrogen bonding to wetting liquids that have the ability to donate electron density (Lewis base). The base component, on the other hand, will characterize how the surface is favorable to accept electron density (Lewis acid). Firstly, a liquid with only dispersive forces is used to determine the contact angle then, two more liquids are necessary to calculate the acid and base components of the surface energy.

Raman

The complete measurement set for all the substrates not presented in the main paper are here illustrated in Fig. S2.

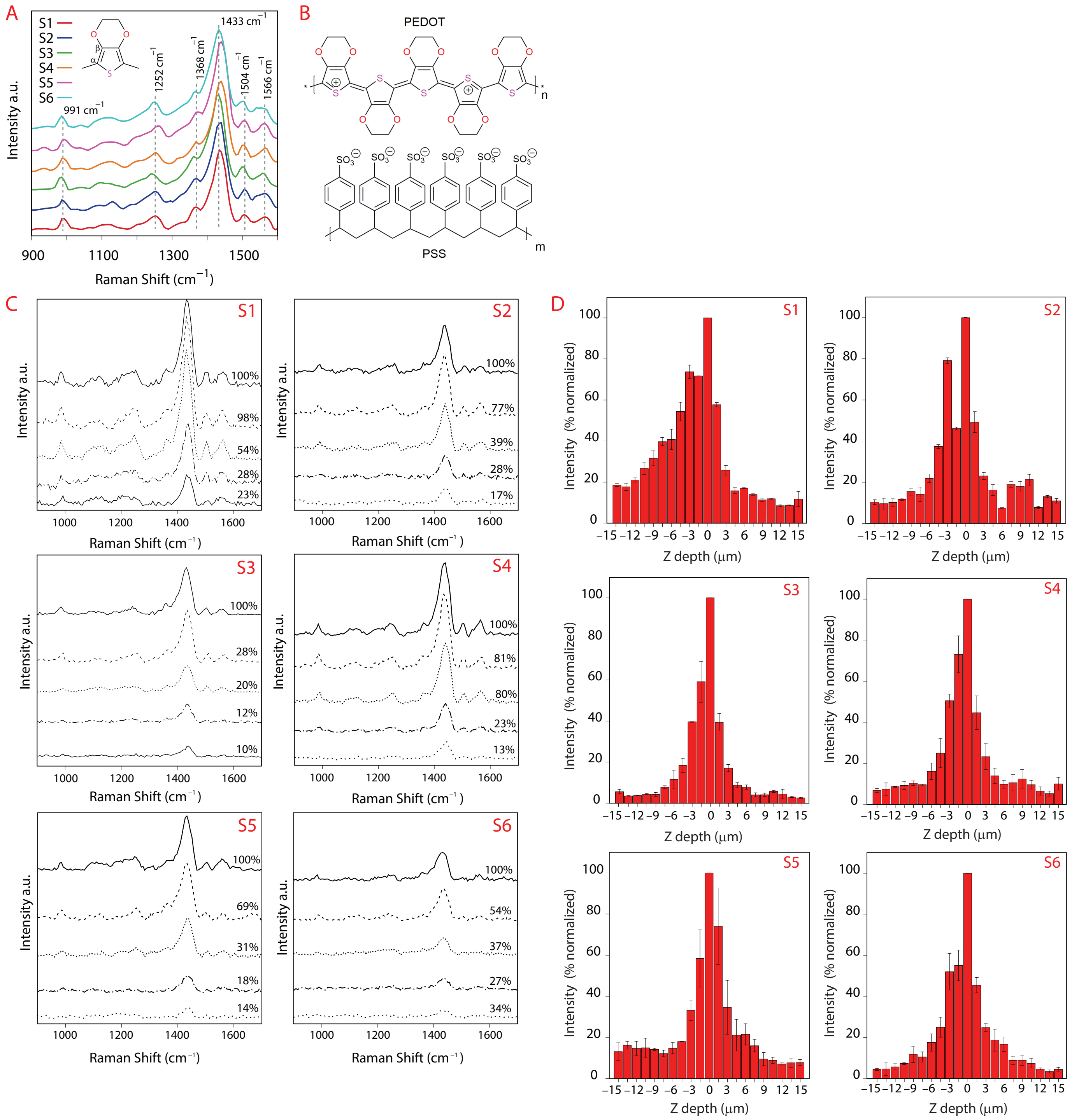

Fig. S2 (A) Raman spectra of the printed PEDOT:PSS ink onto the substrates indicating the vibration frequency of the characteristic bands that is the symmetric stretch at $1433\,\mathrm{cm}^{-1}$ ($C_\alpha = C_\beta$) and the asymmetric stretch ($C = C - O$) at $1504\,\mathrm{cm}^{-1}$. These curves have been normalized at the $991\,\mathrm{cm}^{-1}$ band. (B) Chemical structure of PEDOT:PSS. (C) Raman YZ laser penetration analyses for S1 to S6 indicating the 5 spectra with the highest intensity from the focus point. This curves were not normalized. (D) Raman YZ profile of printed PEDOT:PSS ink ranging from $15\,\mu\mathrm{m}$ above and below the focus point. The negative values indicate the position in the YZ direction above the focus, zero indicates the position of the focus point and the positive ones below focus. We evaluated the band at $1504\,\mathrm{cm}^{-1}$ and the area within the frequency $1379\,\mathrm{cm}^{-1}$ - $1482\,\mathrm{cm}^{-1}$ corresponding to the width of this band

Microscopy images for the printed lines

Images not illustrated in the main paper are illustrated in Fig. S3.

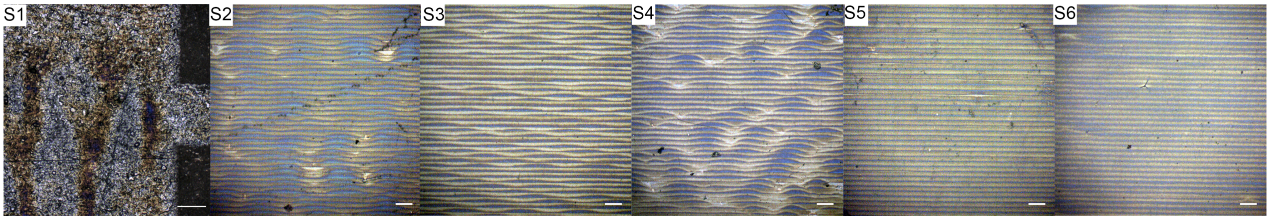

Fig. S3 Microscopy images using 5x magnification taken from the printed surface using the Raman microscope. The scale bar corresponds to $10\,\mu\mathrm{m}$

Influence of sintering

In the main paper we present the results for the influence of sintering of the printed lines for S1, here are the results for the other substrates illustrated in Fig. S4.

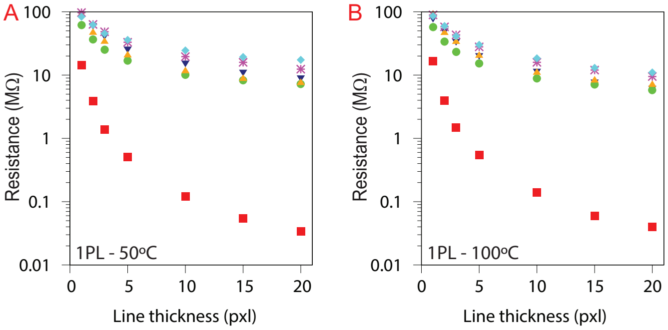

Fig. S4 Effect of sintering at $50\,^{\circ}\mathrm{C}$ and $100\,^{\circ}\mathrm{C}$

Graphene printed on substrate S1 and S2

In order to compare the suitability of the substrates that we used for printing organic PEDOT:PSS inks we printed 2 of the substrates of this study (i.e., S1 and S2) with a graphene ink. This layered material ink is commercially available (Cambridge graphene ltd, Versarien PLC). We used the Dimatix 2831 printer with Dimatix 11610 cartriges. It was necessary to print multilayers of the ink to cover the substrate and get a conductive line. We print 20 layers using two different resolutions (i.e., drop spacing $20\,\mu\mathrm{m}$ and $10\,\mu\mathrm{m}$). The substrate S1 we only print with $20\,\mu\mathrm{m}$ drop spacing and we could not achieve a conductivity line on this sample, on the other hand, we could measured the resistance on the samples printed on S2 and they were $103{\pm}10\,\mathrm{K}\Omega/\mathrm{sq}$ and $14{\pm}2\,\mathrm{K}\Omega/\mathrm{sq}$ for $20\,\mu\mathrm{m}$ and $10\,\mu\mathrm{m}$ respectively for $20\,\mathrm{pxl}$ lines and $174{\pm}1\,\mathrm{K}\Omega/\mathrm{sq}$ and $55{\pm}5\,\mathrm{K}\Omega/\mathrm{sq}$ for $15\,\mathrm{pxl}$ lines. These print outs are illustrated in Fig. S5.

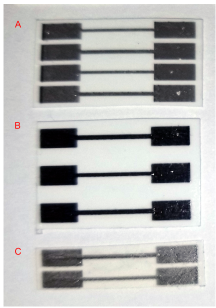

Fig. S5 Printed graphene lines on substrate S2 (A) $20\,\mu\mathrm{m}$ drop spacing with first line thickness $15\,\mathrm{pxl}$ and second line $20\,\mathrm{pxl}$ printed twice and (B) $10\,\mu\mathrm{m}$ drop spacing with first line thickness $20\,\mathrm{pxl}$, middle line $15\,\mathrm{pxl}$ and third line $20\,\mathrm{pxl}$. (C) Printed graphene lines on substrate S1 with first line thickness $20\,\mathrm{pxl}$ and second line $15\,\mathrm{pxl}$ printed with $20\,\mu\mathrm{m}$ drop spacing

Profilometry of the printed lines

An optical profilometry CountourGT (Bruker) based on non-contact vertical scanning interferometry using a 20x magnification Mirau objective and the analysis software Vision64 (Bruker) was used to estimate the thickness of the printed layer on the substrate S3 (see Fig. S6) with not so much success as the layers were very thin and part of the ink was also absorbed by the substrate. Please refer to the literature[10] where we performed these measurements on glass and on substrate S2 using the same ink and conditions as we used in our experiments. On glass the thickness of the layer was $106 \pm 4\,\mu\mathrm{m}$ and on S2 $45 \pm 1\,\mu\mathrm{m}$. This value may be useful to estimate the conductivity of the printed lines based on the resistance measurement and the equation of resistivity, which is the reciprocal of the conductivity. Profilometry of the printed $20\,\mathrm{pxl}$ graphene line is presented in Fig. S7.

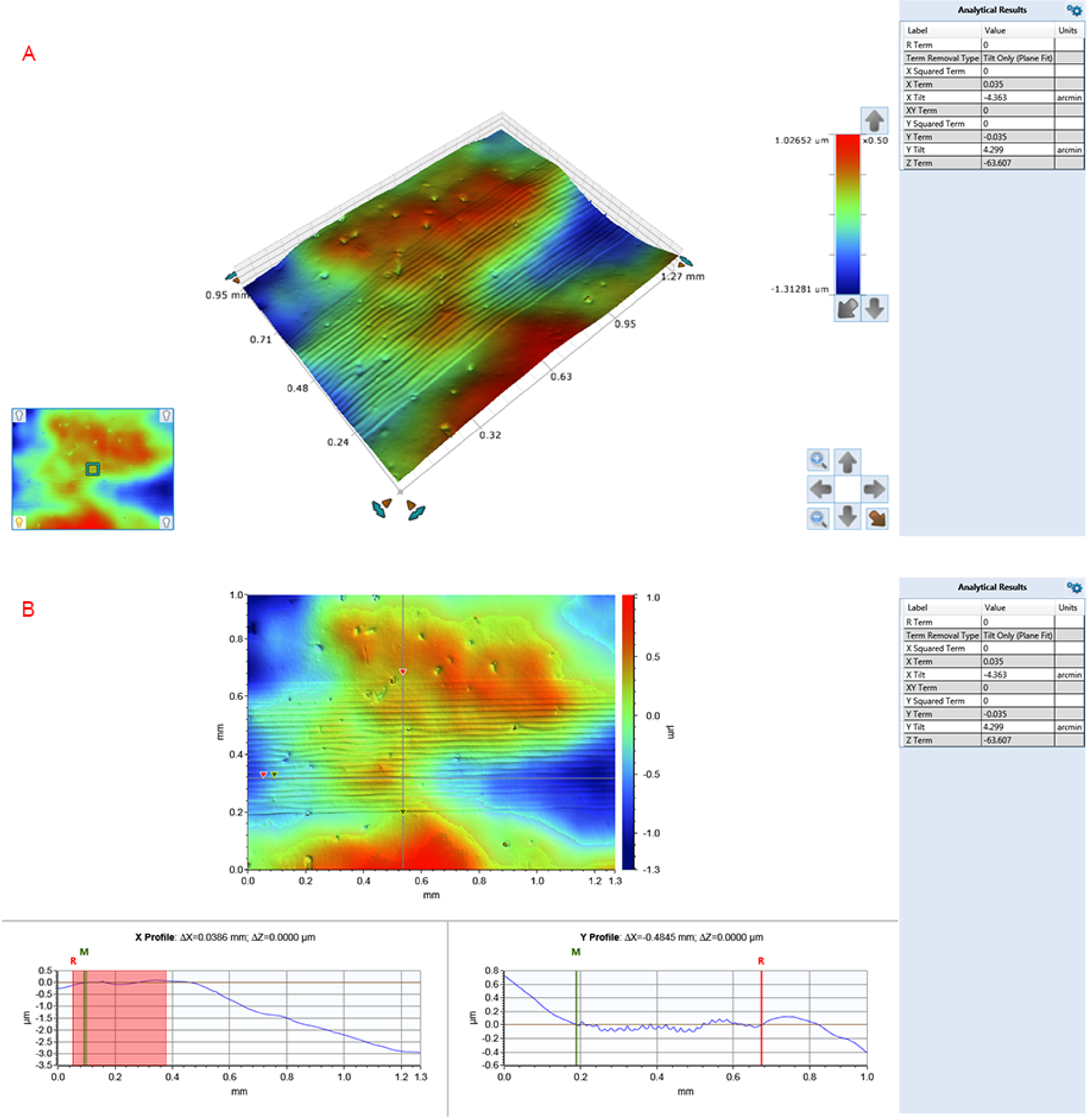

Analytical Results

Label	Value	Units
R Term	0	
Term Removal Type	Tilt Only (Plane Fit)	
X Squared Term	0	
X Term	0.035	
X Tilt	-4.363	arcmin
XY Term	0	
Y Squared Term	0	
Y Term	-0.035	
Y Tilt	4.299	arcmin
Z Term	-63.607	

Analytical Results

Label	Value	Units
R Term	0	
Term Removal Type	Tilt Only (Plane Fit)	
X Squared Term	0	
X Term	0.035	
X Tilt	-4.363	arcmin
XY Term	0	
Y Squared Term	0	
Y Term	-0.035	
Y Tilt	4.299	arcmin
Z Term	-63.607	

Fig. S6 (A) Profilometry on the surface of a $20\,\mathrm{pxl}$ printed line on S3 with the profile illustrated in (B)

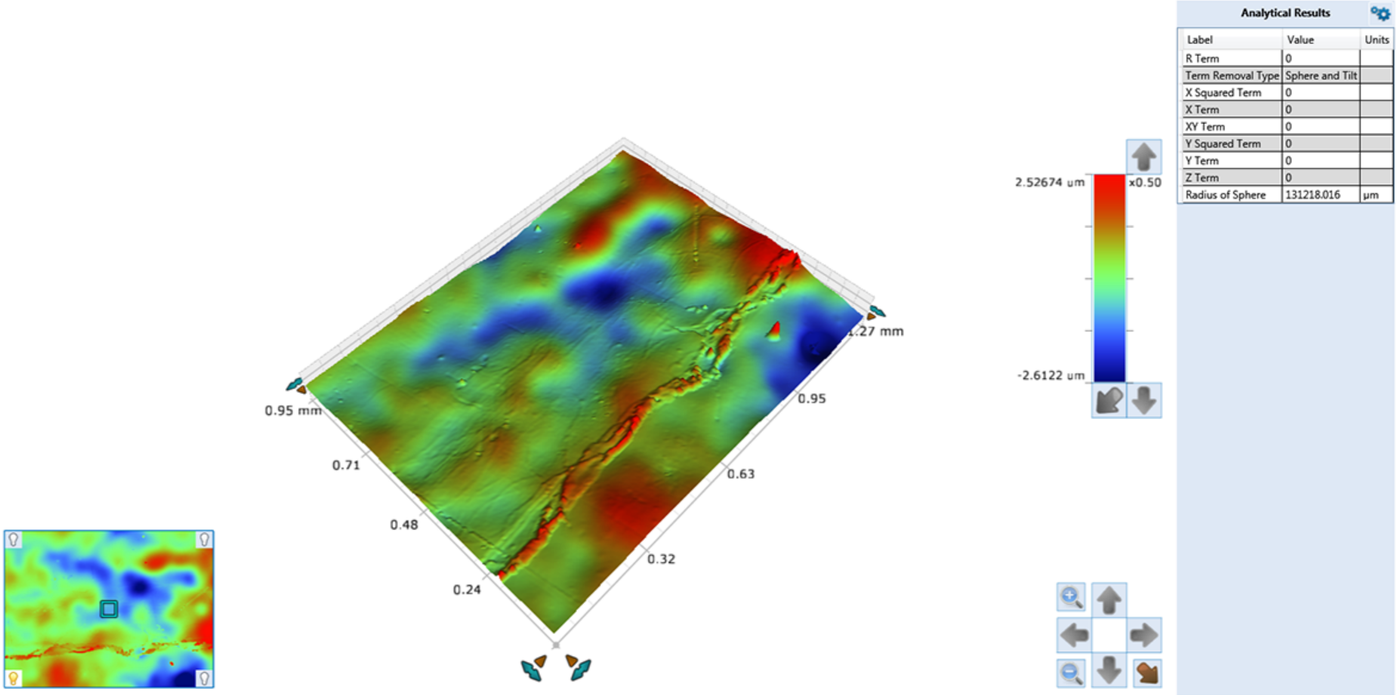

Analytical Results

Label	Value	Units
R Term	0	
Term Removal Type	Sphere and Tilt	
X Squared Term	0	
X Term	0	
XY Term	0	
Y Squared Term	0	
Y Term	0	
Z Term	0	
Radius of Sphere	131218.016	µm

Fig. S7 Profilometry on the surface of $20\,\mathrm{pxl}$ printed line of graphene on S2

ESI References

1 M. Nikolka and H. Sirringhaus, *Conjugated Polymer-Based OFET Devices*, ch. Conjugated Polymers: Properties, Processing, and Applications. CRC Press, 2019.

2 K. Y. Mitra, M. Polomoshnov, C. Martínez-Domingo, D. Mitra, E. Ramon, and R. R. Baumann, “Fully inkjet-printed thin-film transistor array manufactured on paper substrate for cheap electronic applications,” *Advanced Electronic Materials*, vol. 3, no. 12, p. 1700275, 2017.

3 M. M. Hamedi, V. E. Campbell, P. Rothemund, F. Güder, D. C. Christodouleas, J.-F. Bloch, and G. M. Whitesides, “Electrically activated paper actuators,” *Advanced Functional Materials*, vol. 26, no. 15, pp. 2446–2453, 2016.

4 J. Wang, Z. Zheng, H. Li, W. Huck, and H. Sirringhaus, “Dewetting of conducting polymer inkjet droplets on patterned surfaces,” *Nature Materials*, vol. 3, no. 3, p. 171, 2004.

5 C. Wang, H. Dong, W. Hu, Y. Liu, and D. Zhu, “Semiconducting π-conjugated systems in field-effect transistors: A material odyssey of organic electronics,” *Chemical Reviews*, vol. 112, no. 4, pp. 2208–2267, 2012. PMID: 22111507.

6 P. Larkin, *Infrared and Raman spectroscopy: principles and spectral interpretation*. Elsevier, 2017.

7 N. Gierlinger, T. Keplinger, and M. Harrington, “Imaging of plant cell walls by confocal raman microscopy,” *Nature Protocols*, vol. 7, no. 9, p. 1694, 2012.

8 C. J. Van Oss, M. K. Chaudhury, and R. J. Good, “Interfacial lifshitz-van der waals and polar interactions in macroscopic systems,” *Chemical Reviews*, vol. 88, no. 6, pp. 927–941, 1988.

9 T. Carey, C. Jones, F. Le Moal, D. Deganello, and F. Torrisi, “Spray-coating thin films on three-dimensional surfaces for a semitransparent capacitive-touch device,” *ACS Applied Materials & Interfaces*, vol. 10, no. 23, pp. 19948–19956, 2018. PMID: 29745645.

10 J. Mašlík, H. Andersson, V. Forsberg, M. Engholm, R. Zhang, and H. Olin, “Pedot:pss temperature sensor ink-jet printed on paper substrate,” *Journal of Instrumentation*, vol. 13, no. 12, p. C12010, 2018.